Melting of charge/orbital ordered states in $Nd_{1/2}Sr_{1/2}MnO_3$: Temperature and magnetic-field-dependent optical studies

J. H. Jung, H. J. Lee, and T. W. Noh
Department of Physics and Center for Strongly Correlated Materials Research, Seoul National University, Seoul 151-742, Korea

E. J. Choi
Department of Physics, University of Seoul, Seoul 130-743, Korea

Y. Moritomo
CIRSE, Nagoya University, Nagoya 464-8603, Japan
and PRESTO, JST, Japan

Y. J. Wang and X. Wei
National High Magnetic Field Laboratory at Florida State University, Tallahassee, Florida 32310
(Received 27 December 1999)

We investigated the temperature ($T=15\sim290$ K) and the magnetic-field-dependent ($H=0\sim17$ T) optical conductivity spectra of a charge-orbital-ordered manganite $Nd_{1/2}Sr_{1/2}MnO_3$. With variation of T and H, large spectral weight changes were observed up to 4.0 eV. These spectral weight changes could be explained using the polaron picture. Interestingly, our results suggested that some local ordered state might remain above the charge ordering temperature, and that the charge/orbital melted state at a high magnetic field (i.e., at $H=17$ T and $T=4.2$ K) should be a three-dimensional ferromagnetic metal. We also investigated the first order phase transition from the charge-orbital- ordered state to ferromagnetic metallic state using the T- and H-dependent dielectric constants ε. Through the analysis of ε using an effective medium approximation, we found that the melting of charge-orbital-ordered states should occur through the percolation of ferromagnetic metal domains.

I. INTRODUCTION

Doped manganites, with chemical formula $R_{1-x}A_xMnO_3$ [R=La,Nd,Pr, and A=Ca,Sr,Ba], have attracted lots of attention due to their exotic transport and magnetic properties, such as colossal magnetoresistance.[1] The coexistence of ferromagnetism and metallicity, for the samples near $x\sim0.3$, had been explained by the double exchange model.[2] However, it was found that the double exchange interaction alone cannot explain the colossal magnetoresistance.[3] Additional mechanisms were proposed. Among them, two scenarios attracted most of attention: the polaron due to the Jahn-Teller distortion of Mn^{3+} ion[3,4] and the orbital fluctuation.[5,6]

On the other hand, some manganite samples with small bandwidths near $x\sim1/2$ show intriguing charge ordering phenomena,[7] i.e., real space orderings of the Mn^{3+} and the Mn^{4+} ions. For manganites, the charge ordering is usually accompanied with orbital and antiferromagnetic ordering. For example, charge ordering in $Nd_{1/2}Sr_{1/2}MnO_3$ leads to the $d_{3x^2-r^2}(d_{3y^2-r^2})$ orbital ordering and the CE-type antiferromagnetic spin ordering at a low temperature.[8] Moreover, it was found that some charge ordered states could be changed into ferromagnetic metallic states at a higher temperature and/or under a high magnetic field.[8,9] The transitions from charge-orbital-ordered insulator to ferromagnetic metal are usually called ''melting'' of charge-orbital-ordered states.

There have been numerous optical investigations which tried to understand basic mechanisms of colossal magnetoresistance.[10–12] However, only a few works have been reported for optical responses of the charge-orbital-ordered state.[13–15] Recently, Okimoto *et al.* reported the magnetic-field-dependent optical conductivity for a charge-orbital-ordered manganite, $Pr_{0.6}Ca_{0.4}MnO_3$, and that the optical responses under the magnetic field could be understood qualitatively in terms of an insulator-metal transition.[16] However, their measured spectral region was rather limited (i.e., from midinfrared to visible), so details of the insulator-metal transition could not be addressed.

In this paper, we will report optical properties of $Nd_{1/2}Sr_{1/2}MnO_3$. To get clear understanding on the insulator-metal transitions due to the melting of the charge-orbital-ordered states, optical spectra were taken by varying either temperature (T) or magnetic field (H). Our experimental data will be analyzed in terms of the polaron scenario. The changes of the optical response due to the melting of the charge-orbital-ordered states will be explained in terms of the percolation model.

II. EXPERIMENTS

$Nd_{1/2}Sr_{1/2}MnO_3$ single crystal was grown by the floating zone methods. Details of sample growth and characterization were reported elsewhere.[17] The T-dependent resistivity was measured by the four-probe method and the magnetoresistance was obtained using the 20 T superconducting magnet. For optical measurements, the crystal was polished up to 0.3 μm using the diamond paste. To remove surface damages due to the polishing process, we carefully annealed the

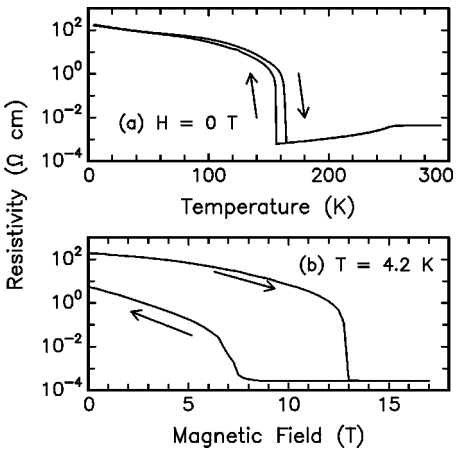

FIG. 1. (a) *T*- and (b) *H*-dependent dc resistivity of $Nd_{1/2}Sr_{1/2}MnO_3$.

sample again in an O_2 atmosphere at 1000 °C just before optical measurements.[18]

Near normal incident reflectivity spectra were measured from 5 meV to 30 eV.[19] A Fourier transform spectrophotometer was used for 5 meV~0.8 eV, and a grating monochromator was used for 0.6~7.0 eV. Above 6 eV, we used the synchrotron radiation from the Normal Incidence Monochromator beam line at the Pohang Light Source. After the spectra were taken, the gold normalization technique was used to subtract surface scattering effects. In the frequency region of 5 meV~4 eV, the *T*-dependent reflectivity spectra were taken using the liquid-He cooled cryostat. In the same frequency region, the *H*-dependent reflectivity spectra were taken with spectrophotometers at National High Magnetic Field Laboratory.

The Kramers-Kronig analyses were used to obtain optical conductivity spectra $\sigma(\omega)$ and dielectric constant spectra $\varepsilon(\omega)$. For these analyses, the room-temperature reflectivity spectrum in the frequency region of 4–30 eV was smoothly connected. Then, the reflectivity at 30 eV was extended up to 40 eV, above which ω^{-4} dependence was assumed. In the low-frequency region, the reflectivity spectrum below 5 meV was extrapolated to be a constant for an insulating state or using the Hagen-Rubens relation for a metallic state.[20] To check the phase errors due to the extrapolations in the Kramers-Kronig analyses, we also independently measured optical constants in the frequency region of 1.5–5 eV using a spectroscopic ellipsometry. It was found that the data from the spectroscopic ellipsometry measurements agreed quite well with the Kramers-Kronig analyses results, demonstrating the validity of our extrapolations.

III. DATA AND RESULTS

A. dc resistivity

Figure 1(a) shows the *T*-dependent dc resistivity curve of $Nd_{1/2}Sr_{1/2}MnO_3$ which was taken with $H=0$ T. With decreasing *T*, the dc resistivity value slightly decreases below the ferromagnetic ordering temperature T_C (~250 K), but it increases abruptly near the charge ordering temperature T_{CO} (~150 K). The dc resistivity value at 4.2 K is estimated to be around 200 Ω cm. With increasing *T*, the dc resistivity value smoothly decreases initially and then experiences an abrupt decrease to ~0.6 mΩ cm near 170 K. The dc resistivity values for the heating run are larger than those for the cooling run, suggesting that the melting of the charge-orbital-ordered states has the nature of first order phase transition. Above 170 K, the dc resistivity values are nearly the same as those for the cooling run. Note that no apparent hysteresis can be observed near T_C.

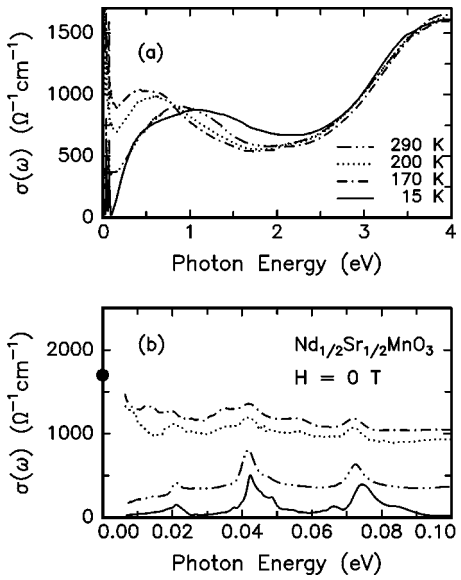

FIG. 2. *T*-dependent $\sigma(\omega)$ of $Nd_{1/2}Sr_{1/2}MnO_3$ below (a) 4.0 eV and (b) 0.1 eV. In (b), the solid circle represents the dc conductivity value at 170 K.

Figure 1(b) shows the *H*-dependent dc resistivity curve of $Nd_{1/2}Sr_{1/2}MnO_3$ which was taken at 4.2 K. With increasing *H*, the dc resistivity value slowly decreases initially, but it suddenly decreases to ~0.2 mΩ cm near 13 T. Above 13 T, the dc resistivity value does not change at all within our experimental errors. With decreasing *H*, the dc value does not change down to 7.5 T and starts to increase abruptly near 7.5 T. The dc resistivity curve shows a very strong hysteresis below 13 T: the dc resistivity values for the field-decreasing run are quite smaller than those for the field-increasing run. Note that the dc resistivity value (~0.2 mΩ cm) for the ferromagnetic metal state at $H=17$ T is lower than that (~0.6 mΩ cm) for the same state at 170 K.

B. Temperature-dependent optical conductivity spectra

The *T*-dependent $\sigma(\omega)$ of $Nd_{1/2}Sr_{1/2}MnO_3$ are shown in Fig. 2(a). At room temperature (i.e., $T>T_C$), there are two broad peaks near 1.0 and 4.0 eV. When entering into the ferromagnetic metallic state (i.e., $T<T_C$), the broad 1.0 eV peak shifts to a lower energy, which accompanies large spectral weight changes. In addition, there is a small decrease of the spectral weight near 3.0 eV. Interestingly, even at a highly metallic state near 170 K, optical conductivity decreases below 0.5 eV and shows the Drude-like behavior below 0.1 eV. When entering into the charge-orbital-ordered state (i.e., $T<T_{CO}$), the spectral weights move to the opposite direction: namely, from a low- to a high-energy region. The optical conductivity spectrum at this charge-orbital-ordered state shows an opening of optical gap ~0.1 eV.

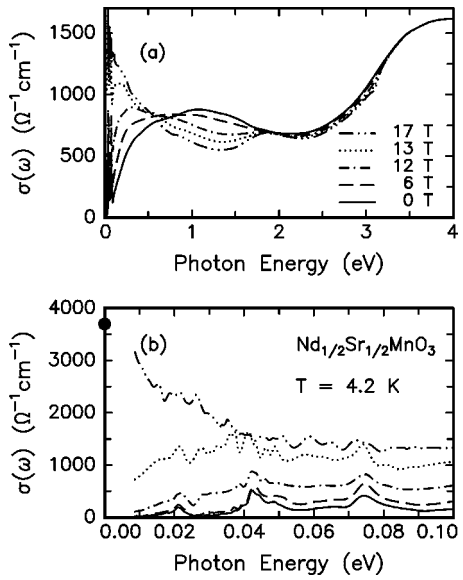

FIG. 3. H-dependent $\sigma(\omega)$ of $Nd_{1/2}Sr_{1/2}MnO_3$ below (a) 4.0 eV and (b) 0.1 eV. In (b), the solid circle represents the dc conductivity value at 17 T.

(This value is in reasonable agreements with the value obtained from recent photoemission experiments.[21]) In addition, the spectral weights near 3.0 eV are restored approximately to the values at $T > T_C$.

The far-infrared $\sigma(\omega)$ are displayed in Fig. 2(b). Above T_C, there are three optical phonon peaks, which are known as the external, the bending, and the stretching modes of the cubic perovskite.[22] In the temperature region of $T_{CO} < T < T_C$, the phonon features are screened and $\sigma(\omega)$ increase significantly. (The solid circle represents the dc conductivity value at 170 K.) Note that the Drude-like absorption behavior is not so clear.[23] Below T_{CO}, $\sigma(\omega)$ decrease quite drastically. At this low temperature, the bending and the stretching modes are splitted and corresponding phonon frequencies move to higher energies. Such changes in the phonon spectra can be understood in terms of the strong lattice distortion due to the charge-orbital ordering.[24]

C. Magnetic-field-dependent optical conductivity spectra

The H-dependent $\sigma(\omega)$, which were taken at 4.2 K, are shown in Fig. 3(a). (Note that the spectra were measured with increasing H.) At 0 T, the optical spectra are nearly the same as those at 15 K, displayed in Fig. 2(a). With increasing H, the spectral weights near 1.2 and 2.7 eV are transferred to lower energy regions. The gap values seem to decrease and finally disappear above 13 T. Note that the H-dependent spectral weight changes are similar to the T-dependent spectral weight changes near T_{CO}. However, the spectra in the ferromagnetic metallic state of 17 T clearly show a Drude-like absorption feature, which is somewhat different from $\sigma(\omega)$ of the ferromagnetic metallic state at 170 K, displayed in Fig. 2(a).

The far-infrared $\sigma(\omega)$ under various H are displayed in Fig. 3(b). At 0 T, the low-temperature phonons can be seen clearly. With increasing H, the phonon peaks become screened and the Drude peak seems to appear above 13 T.

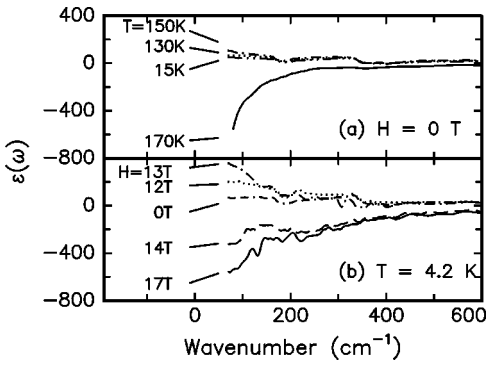

FIG. 4. (a) T- and (b) H-dependent ε of $Nd_{1/2}Sr_{1/2}MnO_3$.

(The solid circle represents the dc conductivity value at 17 T.) Note that the Drude peak becomes clear and appears below 0.04 eV.

D. Behavior of dielectric constants

T-dependent $\varepsilon(\omega)$ is shown in Fig. 4(a). In the insulating state at 15 K, ε is positive and $d\varepsilon/d\omega \approx 0$. With increasing T, ε becomes slightly increased. Above 170 K, it becomes abruptly decreased and $d\varepsilon/d\omega > 0$, which are consistent with typical responses of a metal. Note that the change in ε is rather abrupt near the insulator-metal boundary. Such interesting behaviors of ε can be observed more clearly in the H-dependent $\varepsilon(\omega)$, shown in Fig. 4(b). Up to the insulator-metal phase boundary ($\sim 13\,\mathrm{T}$), ε is increased and then abruptly decreased.

The changes of ε and σ at $100\,\mathrm{cm}^{-1}$ under various H are shown in Figs. 5(a) and 5(b), respectively. These figures show trong hysteresis behaviors. The solid circles and the solid squares represent data during the field-increasing and the field-decreasing runs, respectively. It is clear that the abrupt change in ε occurs near the insulator-metal transition. Note that ε becomes large as the transition region is approached both from the insulating and from the metallic sides.

IV. DISCUSSIONS

A. A schematic diagram of optical transitions

Interpretations on $\sigma(\omega)$ of perovskite manganites have been quite different among experimental groups.[25] However, a correct interpretation is essential to understand physics of

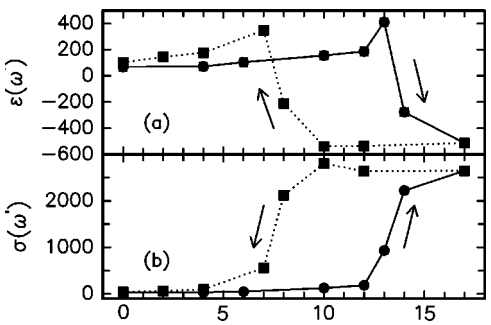

FIG. 5. H dependences of (a) ε and (b) σ at $\omega' = 100\,\mathrm{cm}^{-1}$. The solid and the dotted lines are guides for eye for the field-increasing and the field-decreasing runs, respectively.

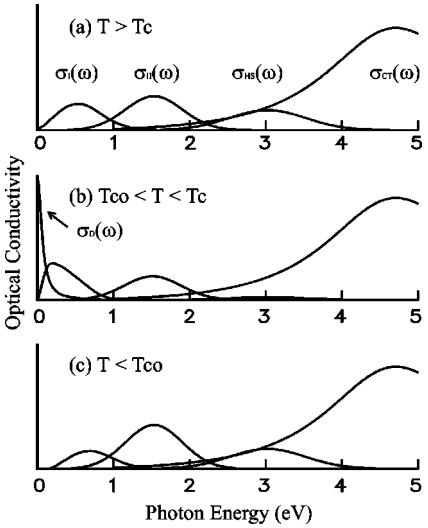

FIG. 6. Schematic diagram of optical transitions for (a) $T > T_C$, (b) $T_{CO} < T < T_C$, and (c) $T < T_{CO}$.

the colossal magnetoresistance and the charge-orbital-ordering phenomena. Recently, we proposed a schematic diagram of $\sigma(\omega)$ based on the polaron scenario,[18,25] which seems to explain most features of optical transitions in colossal magnetoresistance manganites observed by numerous group.[26] We want to extend the schematic diagram to include the charge-orbital-ordered state.

Figure 6 shows our proposed schematic diagram of optical transitions in $Nd_{1/2}Sr_{1/2}MnO_3$: (a) $T > T_C$, (b) $T_{CO} < T < T_C$, and (c) $T < T_{CO}$. Above T_C, there are four main contributions for $\sigma(\omega)$ below 5 eV: (i) $\sigma_I(\omega)$ due to a small polaron absorption below 1.0 eV, (ii) $\sigma_{II}(\omega)$ due to an interorbital transition between the Jahn-Teller splitted levels of the Mn^{3+} ions near 1.5 eV, (iii) $\sigma_{HS}(\omega)$ due to an optical transition between the Hund's rule split bands near 3.0 eV, and (iv) $\sigma_{CT}(\omega)$ due to a charge-transfer transition from the O $2p$ band to the Mn $3d$ band near 4.5 eV. There have been numerous optical reports which support our assignments of the small polaron peak,[27,28] the optical transition between Hund's rule split bands,[29,30] and charge transfer peaks.[10,11,19,28] On the other hand, the existence of peak near 1.5 eV was observed by many workers,[11,28,31] but there remain some controversies for its origin.[32] We think that the most probable candidate is the interorbital transition at the same Mn^{3+} site. Although this transition is prohibited by the selection rule for an Mn atom, this transition could become possible due to the local lattice distortion of MnO_6 octahedra and the strong hybridization between Mn$3d$ and O$2p$ orbitals.

For the ferromagnetic metallic region of $T_{CO} < T < T_C$, the small polaron peak will change into coherent and incoherent absorptions of a large polaron.[12,33] The coherent absorption will appear as Drude-like optical conductivity spectra $\sigma_D(\omega)$ and the incoherent one as an asymmetric midinfrared peak. The increase of electron screening and the decrease of lattice distortion in the metallic state will decrease the 1.5 eV peak somewhat. The optical transition between the Hund's rule splitted bands will decrease, since all of the t_{2g} spins will be aligned in the ferromagnetic state. And, the charge transfer peak remains to be nearly T independent.

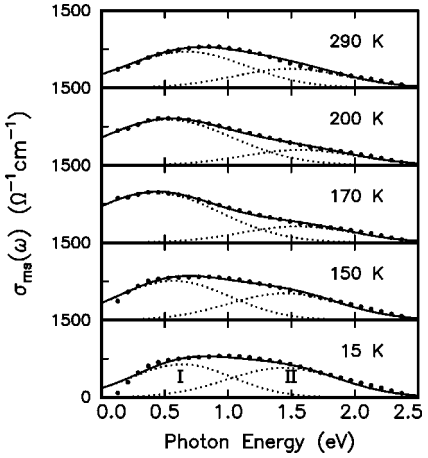

FIG. 7. T-dependent midgap states of $Nd_{1/2}Sr_{1/2}MnO_3$. The solid circles, the dotted lines, and the solid lines represent the experimental data, the Gaussian functions, and the sums of two Gaussian functions, respectively.

Below T_{CO}, the coherent absorption of the free carrier will disappear due to the charge-orbital-ordering. And, its spectrum will be similar to that for $T > T_C$. However, there seems to be three minor but important differences. First, the optical gap due to charge-orbital-ordering should appear. Second, the absorption peak due to the polaron hopping should decrease since such a hopping requires more energy in the antiferromagnetic state. Third, the 1.5 eV peak should become stronger, since lattice distortion becomes larger in the charge-orbital-ordered state.

B. Temperature-dependent spectral weight changes

For the quantitative analysis of T-dependent electronic structure, we analyzed $\sigma(\omega)$ in terms of five peaks, discussed in Sec. IV. A:

$$\sigma(\omega) = \sigma_D(\omega) + \sigma_I(\omega) + \sigma_{II}(\omega) + \sigma_{HS}(\omega) + \sigma_{CT}(\omega). \quad (1)$$

For $\sigma_{HS}(\omega)$ and $\sigma_{CT}(\omega)$, the Lorentzian functions were used. The simple Drude formula were used for $\sigma_D(\omega)$. After subtracting the Drude and high frequency peaks in $\sigma(\omega)$, we obtained the T-dependent midgap component $\sigma_{ms}(\omega)[=\sigma_I(\omega)+\sigma_{II}(\omega)]$. Note that the polaron absorption and the interorbital transition between Mn^{3+} sites are assigned as peak I and peak II, respectively.

Peaks I and II were fitted with two Gaussian functions, as shown in Fig. 7. The solid circles represent the experimental $\sigma(\omega)$ after subtracting $\sigma_{HS}(\omega)$, $\sigma_{CT}(\omega)$, and $\sigma_D(\omega)$. The fitting results with the Gaussian functions could explain the experimental data quite well. Using the integration of each Gaussian function, we derived the T-dependent optical strengths, S_I and S_{II}, for peak I and II, respectively. We also obtained the strength of the Drude weight S_D by integrating the corresponding Drude peak.

The T dependences of S_I, S_{II}, and S_D are displayed in Figs. 8(a), 8(b), and 8(c), respectively. The total spectral weights due to polaron absorption $S_{tot}(=S_I+S_D)$, are also plotted in Fig. 8(d). With decreasing T, S_I starts to increase below T_C and abruptly decreases below T_{CO}. The T dependence of S_{II} is nearly opposite to that of S_I. The T depen-

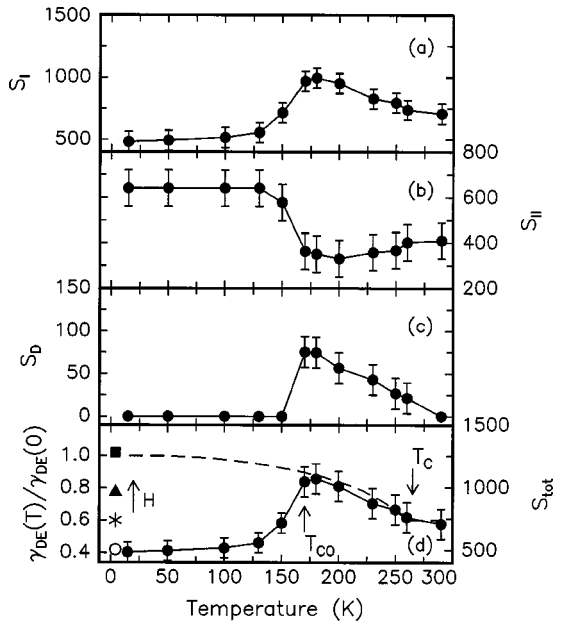

FIG. 8. T-dependent optical strengths (a) S_{I}, (b) S_{II}, (c) S_D, and (d) S_{tot}. (All units are $\Omega^{-1}\,\mathrm{cm}^{-1}\,\mathrm{eV}$.) In (d), the dashed line represents the prediction from the T-dependent double exchange bandwidth. The open circle, the asterisk, the solid triangle, and the solid square represent the S_{tot} at 0, 12, 13, and 17 T, respectively.

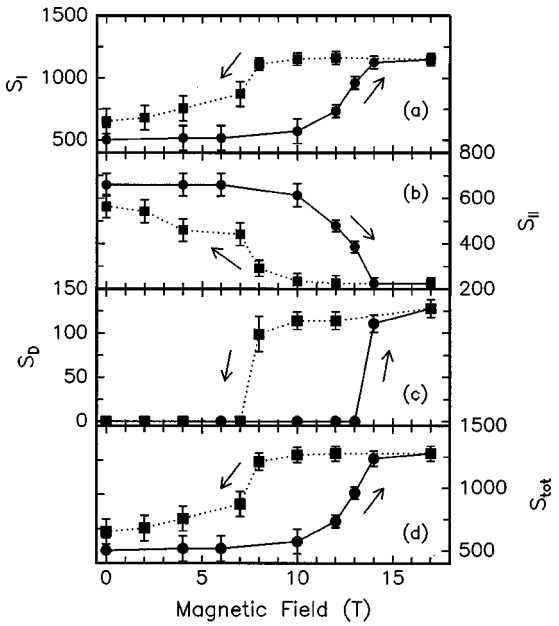

FIG. 9. H-dependent optical strengths (a) S_{I}, (b) S_{II}, (c) S_D, and (d) S_{tot}. (All units are $\Omega^{-1}\,\mathrm{cm}^{-1}\,\mathrm{eV}$.) The solid and the dotted lines are guides for eye for the field-increasing and the field-decreasing runs, respectively.

dence of S_D is similar to S_{I}, but becomes zero for $T < T_{\mathrm{CO}}$. And, S_{tot} starts to increase below T_C and abruptly decreases below T_{CO}. When the sample becomes ferromagnetic below T_C, it becomes metallic. Then, the polaron hopping contribution S_{I} and the free carrier contribution S_D should increase due to the alignment of t_{2g} spins. Due to the increase of metallicity, the lattice distortion of the MnO_6 octahedron will become reduced, resulting in decrease of S_{II}. When the sample becomes antiferromagnetic below T_{CO}, the polaron hopping requires more energy and S_{I} should decrease. The reduction of the metallicity makes S_{II} increase and S_D become zero very rapidly. These temperature dependences are explained using the schematic diagram in Fig. 6.

According to the polaron picture, the T dependence of S_{tot} can be explained more quantitatively. In $(La,Pr)_{0.7}Ca_{0.3}MnO_3$, whose ground state is a three-dimensional ferromagnetic metal, it was found that S_{tot} could be scaled with the T-dependent double exchange bandwidth $\gamma_{\mathrm{DE}}(T)$:[34]

$$\gamma_{\mathrm{DE}} = \langle \cos(\theta_{ij}/2) \rangle, \tag{2}$$

where θ_{ij} is the relative angle of neighboring spins and $\langle\rangle$ represents thermal average in the double exchange model.[35] This scaling behavior was explained in a model by Röder *et al.*[4] where the double exchange and the Jahn-Teller polaron Hamiltonian were taken into account. The dashed line shows $\gamma_{\mathrm{DE}}(T)$ for the three-dimensional ferromagnet. Above T_{CO}, the agreement between $S_{\mathrm{tot}}(T)$ and $\gamma_{\mathrm{DE}}(T)$ is quite good.

However, $S_{\mathrm{tot}}(T)$ deviates from $\gamma_{\mathrm{DE}}(T)$ below T_{CO}. This deviation might be explained by a strong suppression of polaron absorption due to the CE-type antiferromagnetic ordering at the low-temperature region. In the CE-type configuration, the e_g conduction electrons are allowed to hop along the ferromagnetically aligned zigzag chains forming an effective one-dimensional ferromagnet. In the three-dimensional ferromagnet above T_{CO}, the polaron hopping is allowed to six neighboring Mn sites with parallel spins. But, in the one-dimensional ferromagnetic chain, the polaron hopping is allowed only along the zigzag chain. Therefore, the transition from the three-dimensional ferromagnet to the one-dimensional zigzag chain will strongly suppress the polaron absorption near T_{CO}.

C. Magnetic-field-dependent spectral weight changes

With the fitting process used in Sec. IV B, we obtained H-dependent changes of S_{I}, S_{II}, S_D, and S_{tot}, at 4.2 K. Figure 9 shows the results of such fittings, and all of the optical strengths show strong hysteresis behaviors. During the field-increasing run, S_{I} increases near 13 T and becomes nearly saturated above 14 T. During the field-decreasing run, S_{I} remains nearly the same down to 8 T and then abruptly decreases. Note that the value of S_{I} at $H=0$ T after the completion of one cycle is larger than the initial value of S_{I}. The H dependence of S_{II} is nearly opposite to that of S_{I}, but the H dependence of S_{tot} is similar to that of S_{I}. Contrary to rather smooth changes of S_{I}, S_{II}, and S_{tot}, the change of S_D is rather abrupt: the value of S_D becomes nearly zero below 13 T for field-increasing run and below 7 T for field-decreasing run. Qualitatively, the H dependences of S_{I}, S_{II}, and S_D, are quite similar to the T dependences of the corresponding strengths below T_{CO}. These H dependences can be also explained using the schematic diagram in Fig. 6.

Values of S_{tot} at 4.2 K with various values of H were shown in Fig. 8(d). The open circle, the asterisk, the solid triangle, and the solid square represent values of S_{tot} at 0, 12, 13, and 17 T, respectively. With increasing H, S_{tot} increases. At 17 T, it finally reaches the value predicted by Eq. (2) for

the three-dimensional case. This result indirectly supports the fact that the charge-orbital melted state might be a three-dimensional ferromagnetic metal. Note that the value of S_{tot} ($T=170$ K, $H=0$ T) is by about 20% smaller than that of S_{tot} ($T=4.2$ K, $H=17$ T). This experimental fact is consistent with recent magnetostriction measurement[36] and transmission electron microscopy work[37] that there exists a local charge-orbital ordering even above T_{CO}.

D. Percolative phase transition

To get a better understanding on the insulator-metal transition in $Nd_{1/2}Sr_{1/2}MnO_3$, we reexamined $\varepsilon(\omega)$, shown in Sec. III. D. The divergence of ε near the insulator-metal transition has appeared in some materials of the first order transition. For example, it was found that VO_2 films experienced an insulator-metal transition of the first order nature around 70 °C, and that their midinfrared properties could be explained by a composite medium model which takes into account the evolution of domain growth during the first order phase transition.[38] In the composite medium model, the increase of ε near the insulator-metal transition can be interpreted as a dielectric anomaly related to percolation. Therefore, we decided to apply the effective medium approximation (EMA), which is a composite medium model predicting a percolation transition.

In EMA, it is assumed that individual grains, either metallic or insulating, are considered to be embedded in a uniform background, i.e., an ''effective medium'' which has average properties of the mixture.[38,39] A self-consistent condition such that the total depolarization field inside the inhomogeneous medium is equal to zero leads to a quadratic equation for an effective dielectric constant $\tilde{\varepsilon}_{\text{eff}}$,

$$f_i \frac{\tilde{\varepsilon}_i - \tilde{\varepsilon}_{\text{eff}}}{\tilde{\varepsilon}_i + 2\tilde{\varepsilon}_{\text{eff}}} + f_m \frac{\tilde{\varepsilon}_m - \tilde{\varepsilon}_{\text{eff}}}{\tilde{\varepsilon}_m + 2\tilde{\varepsilon}_{\text{eff}}} = 0, \tag{3}$$

where $\tilde{\varepsilon}_i (\equiv \varepsilon_i + i4\pi\sigma_i/\omega)$ and $\tilde{\varepsilon}_m$ represent the complex dielectric constants of the insulating and the metallic $Nd_{1/2}Sr_{1/2}MnO_3$ phases, respectively. And f_i and $f_m (=1-f_i)$ represent volume fractions of the insulating and the metallic domains, respectively. In EMA, the percolation transition occurs at $f_m = 1/3$.

To apply EMA, we assumed that $\tilde{\varepsilon}_i$ and $\tilde{\varepsilon}_m$ could be represented by the experimental complex dielectric constants at 0 and 17 T, respectively. And, we evaluated $\tilde{\varepsilon}_{\text{eff}}$ for various values of f_m. The predictions of ε_{eff} are shown in Fig. 10. If $f_m < 1/3$ (i.e., in the insulating side), ε_{eff} increases when the insulator-metal transition is approached. If f_m becomes larger than 1/3, the low-frequency value of ε_{eff} suddenly becomes negative. By comparing Fig. 10 with Figs. 4(a) and 4(b), it is clear that the EMA results can explain the T-dependent and the H-dependent ε quite well. It should be noted that the percolation model can also explain the increase of ε near the insulator-metal transition. Near the percolation, effective capacitive coupling between the metallic clusters increase due to an increase of effective area and the decrease of spacing between the metallic clusters. This increase of coupling results in the increase of ε near the percolation transition. Therefore, it can be argued that the insulator-metal transition in $Nd_{1/2}Sr_{1/2}MnO_3$ occurs through a percolative phase transition.

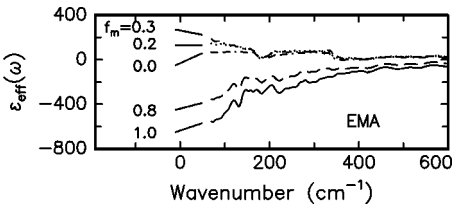

FIG. 10. EMA results of ε_{eff}. Here, f_m represents the volume fraction of the metallic domain.

Recently, there have been lots of studies on the phase separations in doped manganites.[40–46] Our picture of the percolative phase transition agrees with such phase separation. The EMA calculation in Fig. 10 shows that the metallic domain can exist in the insulating states, i.e., below 150 K without H, or below 13 T at 4.2 K. And it also shows that the insulating domain can exist in the metallic states of $Nd_{1/2}Sr_{1/2}MnO_3$. The origin of the phase separations in doped manganites remains controversial. Some workers argue that the phase separation comes from the electronic origin,[44] and some workers argue that it comes from sample inhomogeneity.[45,46] Further studies are required to solve this issue clearly.

V. SUMMARY

We investigated the temperature and the magnetic-field-dependent optical conductivity spectra of charge-orbital-ordered manganite $Nd_{1/2}Sr_{1/2}MnO_3$. By the analyses of the temperature and the magnetic-field-dependent spectral weights, we found that some local-ordered state might remained above the charge-ordering temperature, and that the charge-orbital-melted state at a high magnetic field should be a three-dimensional ferromagnetic metal. Moreover, using the analyses of dielectric constants, we showed that the melting of charge-orbital-ordered states occurred through the percolation in the ferromagnetic metal domains and that optical conductivity should be explained by the two-phase coexistence picture between charge-orbital-ordered insulator and the ferromagnetic metal domains.

ACKNOWLEDGMENTS

We acknowledge Professor J.-G. Park and Dr. K. H. Kim for discussion. We also thank Dr. H. C. Kim and Dr. H.-C. Ri for help in magnetoresistance measurements. This work was supported by the Korea Science and Engineering Foundation through the CSCMR at Seoul National University and by Ministry of Education through the Basic Science Research Institute Program No. BSRI-99-2416. The work by Y.M. was supported by a Grant-in-Aid for Science Research from the Ministry of Education, Science, Sports and Culture, and from PRESTO, JST. Part of this work was performed at the National High Magnetic Field Laboratory, which is supported by NSF Cooperative Agreement No. DMR-9016241 and by the State of Florida.

[1] S. Jin, T.H. Tiefel, M. McCormack, R.A. Fastnacht, R. Ramesh, and L.H. Chen, Science **264**, 413 (1994).
[2] C. Zener, Phys. Rev. **82**, 403 (1951); P.W. Anderson and H. Hasegawa, *ibid.* **100**, 675 (1955).
[3] A.J. Millis, P.B. Littlewood, and B.I. Shraiman, Phys. Rev. Lett. **74**, 5144 (1995).
[4] H. Röder, J. Zhang, and A.R. Bishop, Phys. Rev. Lett. **76**, 1356 (1996).
[5] S. Ishihara, J. Inoue, and S. Maekawa, Phys. Rev. B **55**, 8280 (1997).
[6] F. Mack and P. Horsch, Phys. Rev. Lett. **82**, 3160 (1999).
[7] C.H. Chen and S-W. Cheong, Phys. Rev. Lett. **76**, 4042 (1996); S. Mori, C.H. Chen, and S-W. Cheong, Nature (London) **392**, 473 (1998).
[8] H. Kuwahara, Y. Tomioka, A. Asamitsu, Y. Moritomo, and Y. Tokura, Science **270**, 961 (1995).
[9] Y. Tomioka, A. Asamitsu, H. Kuwahara, Y. Moritomo, and Y. Tokura, Phys. Rev. B **53**, R1689 (1996).
[10] Y. Okimoto, T. Katsufuji, T. Ishikawa, A. Urushibara, T. Arima, and Y. Tokura, Phys. Rev. Lett. **75**, 109 (1995).
[11] M. Quijada, J. Černe, J.R. Simpson, H.D. Drew, K.H. Ahn, A.J. Millis, R. Shreekala, R. Ramesh, M. Rajeswari, and T. Venkatesan, Phys. Rev. B **58**, 16 093 (1998).
[12] K.H. Kim, J.H. Jung, and T.W. Noh, Phys. Rev. Lett. **81**, 1517 (1998).
[13] H.L. Liu, S.L. Cooper, and S-W. Cheong, Phys. Rev. Lett. **81**, 4684 (1998).
[14] P. Calvani, G. De Marzi, P. Dore, S. Lupi, P. Maselli, F. D'Amore, S. Gagliardi, and S-W. Cheong, Phys. Rev. Lett. **81**, 4504 (1998).
[15] J.H. Jung, J.S. Ahn, J. Yu, T.W. Noh, J. Lee, I. Solovyev, and K. Terakura, Phys. Rev. B **61**, 6902 (2000).
[16] Y. Okimoto, Y. Tomioka, Y. Onose, Y. Otsuka, and Y. Tokura, Phys. Rev. B **57**, R9377 (1998); **59**, 7401 (1999).
[17] Y. Moritomo, H. Kuwahara, Y. Tomioka, and Y. Tokura, Phys. Rev. B **55**, 7549 (1997).
[18] H.J. Lee, J.H. Jung, Y.S. Lee, J.S. Ahn, T.W. Noh, K.H. Kim, and S-W. Cheong, Phys. Rev. B **60**, 5251 (1999).
[19] J.H. Jung, K.H. Kim, D.J. Eom, T.W. Noh, E.J. Choi, J. Yu, Y.S. Kwon, and Y. Chung, Phys. Rev. B **55**, 15 489 (1997).
[20] K.H. Kim, J.Y. Gu, H.S. Choi, D.J. Eom, J.H. Jung, and T.W. Noh, Phys. Rev. B **55**, 4023 (1997).
[21] A. Sekiyama, S. Suga, M. Fujikawa, S. Imada, T. Iwasaki, K. Matsuda, T. Matsushita, K.V. Kaznacheyev, A. Fujimori, H. Kuwahara, and Y. Tokura, Phys. Rev. B **59**, 15 528 (1999).
[22] K.H. Kim, J.Y. Gu, H.S. Choi, G.W. Park, and T.W. Noh, Phys. Rev. Lett. **77**, 1877 (1996).
[23] Similar to our results, Saitoh *et al.* [E. Saitoh, Y. Okimoto, Y. Tomioka, T. Katsufuji, and Y. Tokura, Phys. Rev. B **60**, 10 362 (1999)] reported optical spectra for bandwidth controlled $R_{0.6}Sr_{0.4}MnO_3$. For small bandwidth systems, they found that the low-T optical spectrum tends to lose the Drude weight and becomes ω-independent. And they explained such behaviors using the instabilities triggered by small bandwidth.
[24] T. Ishikawa, K. Ookura, and Y. Tokura, Phys. Rev. B **59**, 8367 (1999).
[25] T.W. Noh, J.H. Jung, and K.H. Kim, *Physics of Manganites*, edited by T.A. Kaplan and S.D. Mahanti (Kluwer Academic, New York, 1999), and references therein.
[26] Recently, Mack and Horsch (Ref. 6) made a theoretical prediction on $\sigma(\omega)$ of doped x^2-y^2 ordered phase based on the orbital fluctuation scenario. We measured $\sigma(\omega)$ of $Pr_{1/2}Sr_{1/2}MnO_3$, which is known to have such ordered phase. However, our experimental $\sigma(\omega)$ could not be explained by the orbital fluctuation scenario. [Refer to J. H. Jung, H. J. Lee, J. Yu, T. W. Noh, E. J. Choi, and Y. Moritomo, Phys. Rev. B **61**, 14 656 (2000).]
[27] S.G. Kaplan, M. Quijada, H.D. Drew, D.B. Tanner, G.C. Xiong, R. Ramesh, C. Kwon, and T. Venkatesan, Phys. Rev. Lett. **77**, 2081 (1996).
[28] J.H. Jung, K.H. Kim, T.W. Noh, E.J. Choi, and J. Yu, Phys. Rev. B **57**, R11 043 (1998).
[29] Y. Moritomo, A. Machida, K. Matsuda, M. Ichida, and A. Nakamura, Phys. Rev. B **56**, 5088 (1997).
[30] J.H. Jung, K.H. Kim, H.J. Lee, J.S. Ahn, N.J. Hur, T.W. Noh, M.S. Kim, and J.-G. Park, Phys. Rev. B **59**, 3793 (1999).
[31] A. Machida, Y. Moritomo, and A. Nakamura, Phys. Rev. B **58**, 12 540 (1998).
[32] Quijada *et al.* (Ref. 11) assigned the peak as inter-orbital transition between different Mn^{3+} site. And Machida *et al.* (Ref. 31) assigned it as the optical transition related to Jahn-Teller clusters.
[33] S. Yoon, H.L. Liu, G. Schollerer, S.L. Cooper, P.D. Han, D.A. Payne, S-W. Cheong, and Z. Fisk, Phys. Rev. B **58**, 2795 (1998).
[34] K.H. Kim, J.H. Jung, D.J. Eom, T.W. Noh, J. Yu, and E.J. Choi, Phys. Rev. Lett. **81**, 4983 (1998).
[35] K. Kubo and N. Ohata, J. Phys. Soc. Jpn. **33**, 21 (1972).
[36] R. Mahendiran, M.R. Ibarra, A. Maignan, F. Millange, A. Arulraj, R. Mahesh, B. Raveau, and C.N.R. Rao, Phys. Rev. Lett. **82**, 2191 (1999), and references therein.
[37] N. Fukumoto, S. Mori, N. Yamamoto, Y. Moritomo, T. Katsufuji, C.H. Chen, and S-W. Cheong, Phys. Rev. B **60**, 12 963 (1999).
[38] H.S. Choi, J.S. Ahn, J.H. Jung, T.W. Noh, and D.H. Kim, Phys. Rev. B **54**, 4621 (1996).
[39] T.W. Noh, Y. Song, S.-I. Lee, J.R. Gaines, H.D. Park, and E.R. Kreidler, Phys. Rev. B **33**, 3793 (1986).
[40] S. Yunoki, J. Hu, A.L. Malvezzi, A. Moreo, N. Furukawa, and E. Dagotto, Phys. Rev. Lett. **80**, 845 (1998).
[41] A. Moreo, S. Yunoki, and E. Dagotto, Science **283**, 2034 (1999).
[42] G. Allodi, R. De Renzi, F. Licci, and M.W. Pieper, Phys. Rev. Lett. **81**, 4736 (1998).
[43] M. Fäth, S. Freisem, A.A. Menovsky, Y. Tomioka, J. Aarts, and J.A. Mydosh, Science **285**, 1540 (1999).
[44] M. Uehara, S. Mori, C.H. Chen, and S-W. Cheong, Nature (London) **399**, 560 (1999).
[45] R.H. Heffner, L.P. Le, M.F. Hundley, J.J. Neumeier, G.M. Luke, K. Kojima, B. Nachumi, Y.J. Uemura, D.E. MacLaughlin, and S-W. Cheong, Phys. Rev. Lett. **77**, 1869 (1996).
[46] C.H. Booth, F. Bridges, G.H. Kwei, J.M. Lawrence, A.L. Cornelius, and J.J. Neumeier, Phys. Rev. B **57**, 10 440 (1998).